DISTRIBUTION STATEMENT A: Approved for public release; distribution is unlimited.

New River Inlet DRI: Observations and Modeling of Flow and Material Exchange & Field and Numerical Study of the Columbia River Mouth

Jamie MacMahan[1], Ad Reniers[2], Guy Gelfenbaum[3]

[1]Oceanography Department, Spanagel 327c, Naval Postgraduate School, Monterey, CA 93943
Phone: (831) 656-2379 Fax: (831) 656-2712 Email: jhmacmah@nps.edu
NPS Award Number: (N0001411WX20962; N0001412WX20498; N0001413WX20480)

[2]Rosenstiel School of Marine and Atmospheric Science, Miami, FL33149
Phone: (305) 421-4223 Fax: (305) 421-4701 Email: areniers@rsmas.miami.edu
UM Award Number: (N000141110376, N000141010379, N000141310185)

[3]USGS 400 Natural Bridges Dr., Santa Cruz, CA 95060
Phone: (831) 460-7417 email: ggelfenbaum@usgs.gov

LONG-TERM GOALS

The goal of our effort is to understand river and inlet fluid dynamics through in situ field observations and model validation.

OBJECTIVES

The main objectives of our FY13 effort were to:

- perform a comprehensive field experiment in the Mouth of the Columbia River (MCR) in collaboration with the USGS (Guy Gelfenbaum, amongst others);
- analyze the MCR drifter, in situ mini-catamaran, pressure, and USGS tripod observations;
- describe the tidal chocking behavior at New River Inlet (NRI);
- describe the generation mechanisms for fronts at NRI through observations and modeling;
- evaluate the optical properties of NRI through ins situ observations;
- verify Delft3D in predicting the complex velocity field and concurrent sediment transports under a range of environmental conditions (i.e. waves, wind and potentially stratification)

APPROACH

Our approach is to collect field observations to evaluate the sensitivity of Delft3D at the Mouth of the Columbia River and at New River Inlet, NC.

WORK COMPLETED

We (MacMahan, Reniers, Gelfenbaum, students and technicians) collected various field observations at the MCR in May-June 2013. We are in the midst of analyzing the field data and evaluating Delft3D. We are actively collaborating with PIs involved with RIVET-II effort.

For example during RIVET-II, we deployed GPS-equipped drifters ten times over three weeks on ebb and flood tides. The drifters were deployed at different locations in the MCR including Baker Bay. These drifter deployments were planned with a Delft3D forecast model using the predicted tides, wind, wave and river discharge conditions to optimize spatial coverage and drifter retrieval operations. On June 6 we spatially deployed 90 drifters between the jetties at the onset of flood tide. For this particular day the objective was to map the flood-slack-ebb particle pathways and velocities starting from the jetty entrance. For this successful deployment the forecast and observations show a good match (compare panels in Figure 1).

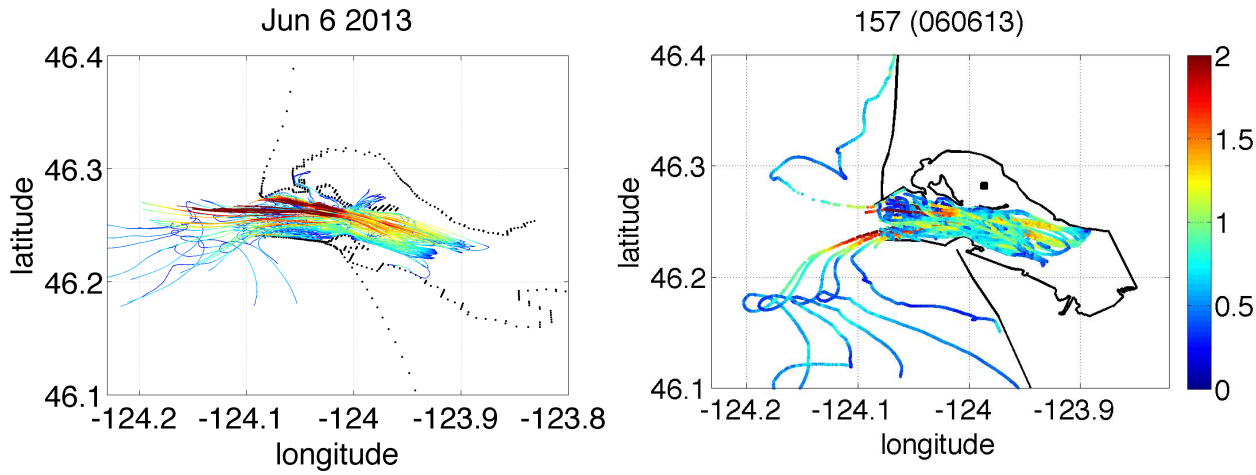

Figure 1. Drifter speed tracks for June 6, 2013 at the Mouth of the Columbia River. The color of the line is the drifter speed. Speed color scale plotted to the right (m/s). Black lines/dots indicate land boundaries. Left panel: Delft3D forecast. Right panel: Observations.

RESULTS

1) Fortnightly tides and subtidal motions at New River Inlet

Observations of an 87% reduction in the amplitude of the semi-diurnal tidal constituent at New River Inlet, NC, suggest that the estuary system is tidally choked. There is a near linear decay in the semi-diurnal amplitude from the ebb-tidal delta to the end of the channel that opens up in the backbay, validating an assumption in previously proposed dynamical tidal models [Keulegan, 1967; Stigebrant, 1980; Hill, 1994]. The inlet behaves as a low-pass hydraulic filter [Kjerfve and Knoppers, 1991], resulting in different backbay amplitude and phase responses for the semi-diurnal, diurnal, subtidal, and fortnightly signals. The observed backbay subtidal and fortnightly surface elevations are not simulated accurately by a monochromatic tidal-choking model (e.g. Keulegan, 1967). In contrast, a simple, non-monochromatic, dimensional model that balances pressure gradients with bottom friction, and that includes a tidally varying water depth and allows nonlinear interactions between constituents predicts accurately the backbay subtidal (Figure 2) and fortnightly response. Numerical experiments demonstrate that there is nonlinear coupling via the quadratic bottom friction primarily between the relatively large M2 tidal constituent and the subtidal and fortnightly ocean signals. The temporal lag of the low-frequency signal is increased with increasing high-frequency (M2) amplitude. The nonlinear coupling between MSF and M2 is important to the fortnightly backbay response. The subtidal and

fortnightly motions transport colder, saline ocean water into the backbay, and increase sea levels in the estuary, and thus the nonlinear coupling between tidal constituents must be considered to predict the subtidal and fortnightly exchange of waters between the backbay and ocean.

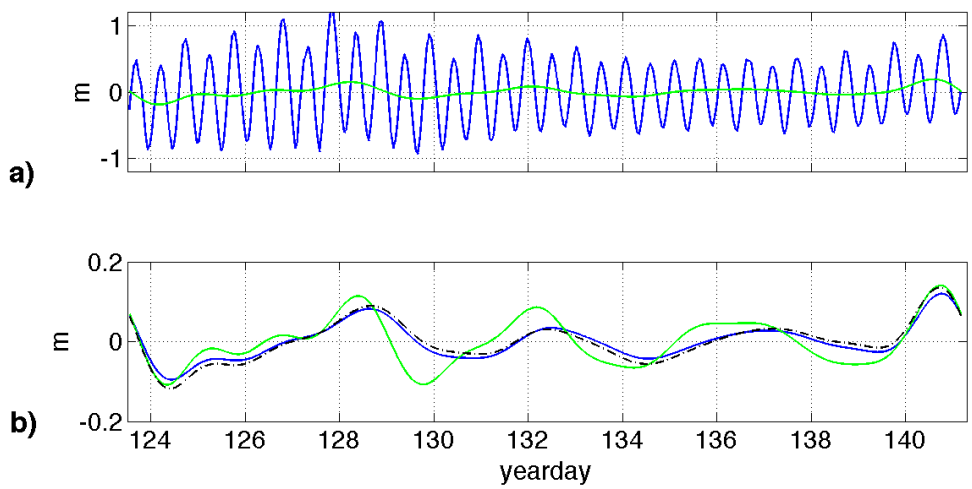

Figure 2. a) Measured ocean sea-surface elevation for the subtidal (green) and the high-frequency tidal constituents (blue), and b) modeled subtidal sea-surface elevation in the backbay for the ocean subtidal signal as model input only (green) and for the subtidal plus high-frequency tidal constituents as model input (blue) versus time. The black dashed curve is the measured subtidal response in the backbay.

2) Tidal Exchange

As part of the RIVET 1 experiment dye was released at the mouth of the inlet during a flood tide to quantify tidal exchange by measuring the flux of dye into and out of the inlet through the primary channel using three fixed measurement stations equipped with ADCPs and dye-sensors. At high water during the release the ocean water flooded the southern channel shoreline causing overwash into the adjacent marshland, including a noticeable amount of dye (Figure 3a). Although the presence of overwash made a direct tidal exchange calculation impossible, it did raise the question of how much flooding water bypasses the primary channel during an overwash event and how does this affect the marshland? To examine this, the percentage of dye that bypasses the primary channel was calculated. To that end a log-fit was performed to the measured velocity profiles (following Faria *et al.,* 1998), resulting in bottom friction coefficient during the flood of $Cf = 0.003$ whereas during the ebb it is $Cf = 0.007$. Although a decrease in friction coefficient is consistent with depth-dependent friction formulations like Manning, these formulations cannot explain the large difference between ebb and flood friction values given the limited tidal depth variation.

This asymmetry in the friction coefficients is currently being examined in more detail with Delft3D (see also section 4 below). Next the transverse logarithmic velocity field was reconstructed based on the flood friction coefficient and local water depth and combined with the dye observations to calculate the dye flux.

We found that during the flood at most 48% of the upstream flux was accounted for downstream with an average value of 37%. When integrated over the entire flood, only an estimated 27% of the total dye released flows past the primary channel transect (Figure 3b). These data are being used to compare with Delft3D calculations to assess the overwash event and it's potential implications for tidal

exchange. To better define the correlation between the physics of the inlet system and the tidal exchange affected by overwash events a new method was developed using virtual tracer technique to calculate residence times of estuarine water. This method is presently being testes and is the topic of ongoing research with results expected by the end of 2013.

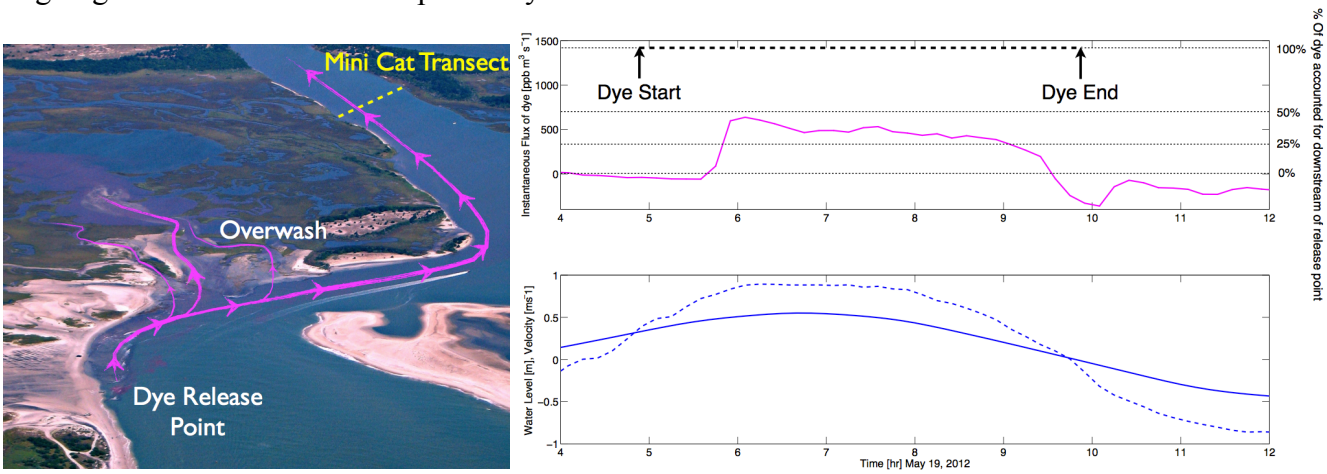

Figure 3. a) Plan view of dye-release on flood (picture courtesy of Gorgon Farquharson and APL-UW). b) Top panel: Calculated dye flux at the mini-cat locations. Bottom panel: Corresponding tidal elevation (solid line) and along-channel velocity (dashed line). Note the reversal in dye flux as the flow starts ebbing.

3) Tidal Intrusion Fronts

Subsurface structure and force balance were analyzed across an axially oriented surface front that reliably forms in the lower estuary inside the New River Inlet at the landward end of the artificially extended (via dredging) main tidal channel. Measurements collected during RIVET I include ADCP and CTD measurements from mini-cats, CTD casts, and surface drifter traces. The analysis included cross-front density and velocity structures (Figure 4a-c.) to describe the front and calculation of Froude balances (inertial vs. buoyant forces, Figure 4d) for classification. The cross sections describe a subsurface structure that persists through the tidal flood and includes subduction at the surface front, a 100-meter-wide stratification zone, and a cross-front circulation cell comprising a densimetric gravity current in the deep, dense layer and a surface return flow that generates the convergence necessary to create the surface front. This behavior is consistent with a tidal intrusion front, and is further supported by its occurrence in the lee of a shoal that acts as a hydraulic control.

The single observational exception to tidal intrusion front behavior is that the surface flows converge at the front in a confluent manner, vice the more direct convergence described in the conceptual model [Largier, 1992]. Froude balances are calculated at each mini-cat location (M131-M134) as a diagnostic measure of whether force balances transition from supercritical on the dense hydraulically controlled side of the front to subcritical in the stratified and less dense side of the front. Owing to the confluence of the flow, the total flow on both sides of the front (Figure 4d, in black) is supercritical, but re-calculating with components parallel (blue) and orthogonal (red) to the front reveals the expected orthogonal transition from supercritical to subcritical coincident with the surface front location. This confirms the front as a bathymetrically induced subduction front and subsurface gravity current, although the confluent flow distinguishes this front strictly from a tidal intrusion front. Crucial in this case to formation of this sort of stratified feature in an otherwise well-mixed estuary is the statistical

distinction of the water mass in Traps Bay shown by Sheets [2013], and the re-introduction of that water to the main tidal flow in the lee of a shoal sufficient to bring the primary flood flow under hydraulic control.

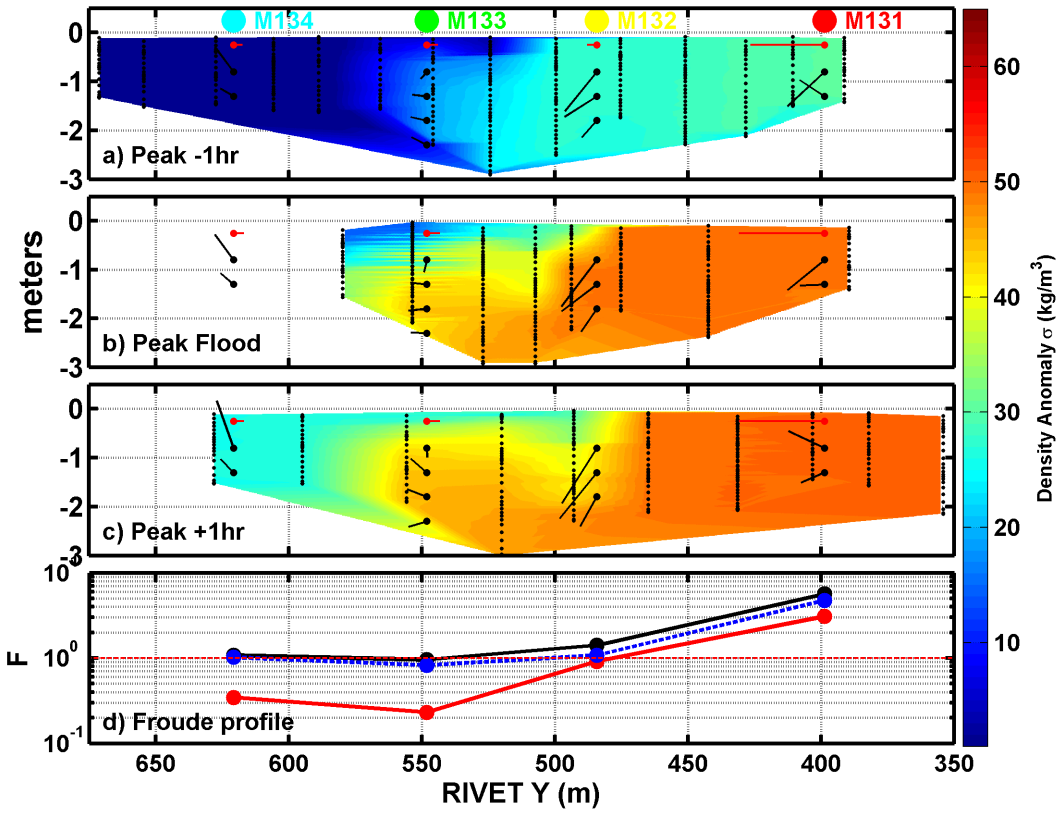

Figure 4. Cross-sections of the front collected on May 13 **(a)** one hour prior, **(b)** near, and **(c)** one hour following offshore high tide, which roughly corresponds to local peak flood. View is seaward, with the main tidal channel on the right hand side and the water exiting Traps Bay on the left hand side. Coloration is density anomaly, linearly interpolated between CTD casts shown as vertical black lines. Black vectors are ADCP velocity profiles at the mini-cat locations shown. Red vectors are cross-front drifter velocities. **(d)** Froude number calculations at each mini-cat location, corresponding to the time of panel (c). Data points are calculated from total (F_t ●), cross-front (F_x ●) and along-front (F_l ●) velocity vectors.

4) 3D tidal currents at New River Inlet

Most tidal modeling efforts use depth-averaged currents (2DH) to calculate the tidal wave propagation into the inlet. For RIVET1 we explore the differences of 3D versus 2DH modeling for the tidal wave propagation using both current velocities measured in the inlet channel (Figure 5) and pressure recordings within the bay. The model boundary conditions include tidal elevation, waves, wind and salinity. The model bathymetry is based on a combination of USACE surveys performed prior and during the field experiment (McNinch et al., 2012), a pre-existing survey of the back bay combined with a post-experiment jet-ski survey in January of 2013 of the back bay area between the ICW and Snead's Ferry as well as walking surveys along the inlet channel and overwash area. All bathymetric data have been translated to Mean Sea Level (MSL) and lat-lon coordinates have been transformed to a local coordinate system for easy reference (Figure 6). The model uses a spatially varying curvilinear

mesh. Bottom friction is modeled with a manning number of 0.028 and a k-e turbulence model combined with HLES (Uittenboogaard, 1998) to calculate vertical and horizontal turbulent eddy viscosities. The 3D model uses 10 sigma layers refined at the bottom and the surface to accommodate bed and wind stress respectively.

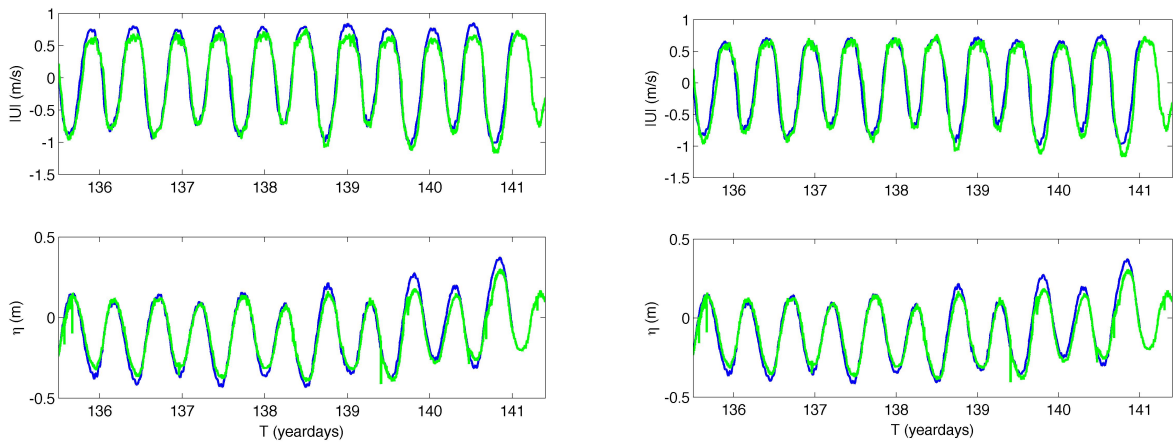

Figure 5. Model calculations (blue) and observations (green) at the minicat location within the inlet channel of the alongchannel velocity (upper panels) and tidal elevation (lower panels). Left panel: 2DH. Right panel: 3D. The mismatch after yearday 139 is due to non-resolved sub-tidal motions (see section 1).

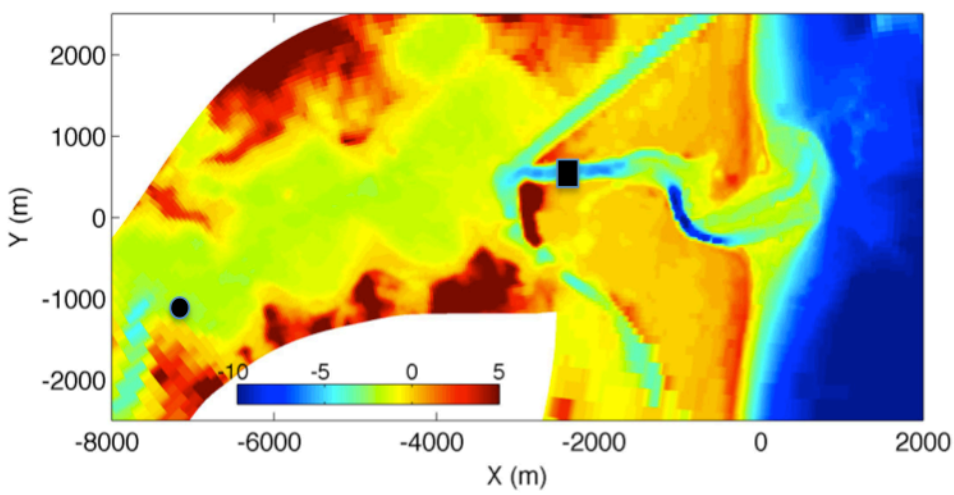

Figure 6. Model bathymetry detail for New River Inlet with bed level in meters indicated by the color scale with mini-cat ADCP locations within the inlet channel (black square) and Sneads Ferry pressure sensor within the back bay (black dot).

Optimal results are obtained for the 3D modeling simulation with a good match at Sneads Ferry (not shown) and at the mini-cat transect in the inlet channel (Figure 5). The asymmetry in along-channel velocities discussed in section *ii* cannot be explained by the 2DH modeling approach, but is matched with the 3D calculations. This has important implications for the ebb-tidal jet as it exits the inlet and therefore mixing and exchange as discussed in section 2 and is the subject of ongoing research.

5) New River Inlet Optical Properties

Spatial and temporal observations of CDOM, salinity and temperature were obtained in New River Inlet, NC to describe the salinity, temperature and optical characterization of a tidally choked estuary with connecting intra-coastal waterways (ICWs). Four different water masses identified as originating from different regions of the estuary, contribute to the characterization of the inlet: 1) ocean (low CDOM, high salinity, and low temperature water), 2) backbay (high CDOM, lower salinity, and warm temperatures), 3) southern ICW (high CDOM, hyper-saline, warm water), and 4) a mixed region (Figure 7). During flood tides, ocean water is transported into the backbay and during ebb tides, backbay water is transported into the ocean. The proximity of the neighboring inlets affects the exchange processes between the southern and northern ICW. The inlet 36km south of New River causes the southern ICW to respond as a tidally choked channel, reducing exchange processes and resulting in increased CDOM, temperature, and salinity. On the contrary, the inlet 12km north of New River Inlet allows free exchange processes between the ocean and the backbay. An interaction exists between the ICWs and the primary inlet tidal channel, where backbay and ocean water are both transported to the ICWs.

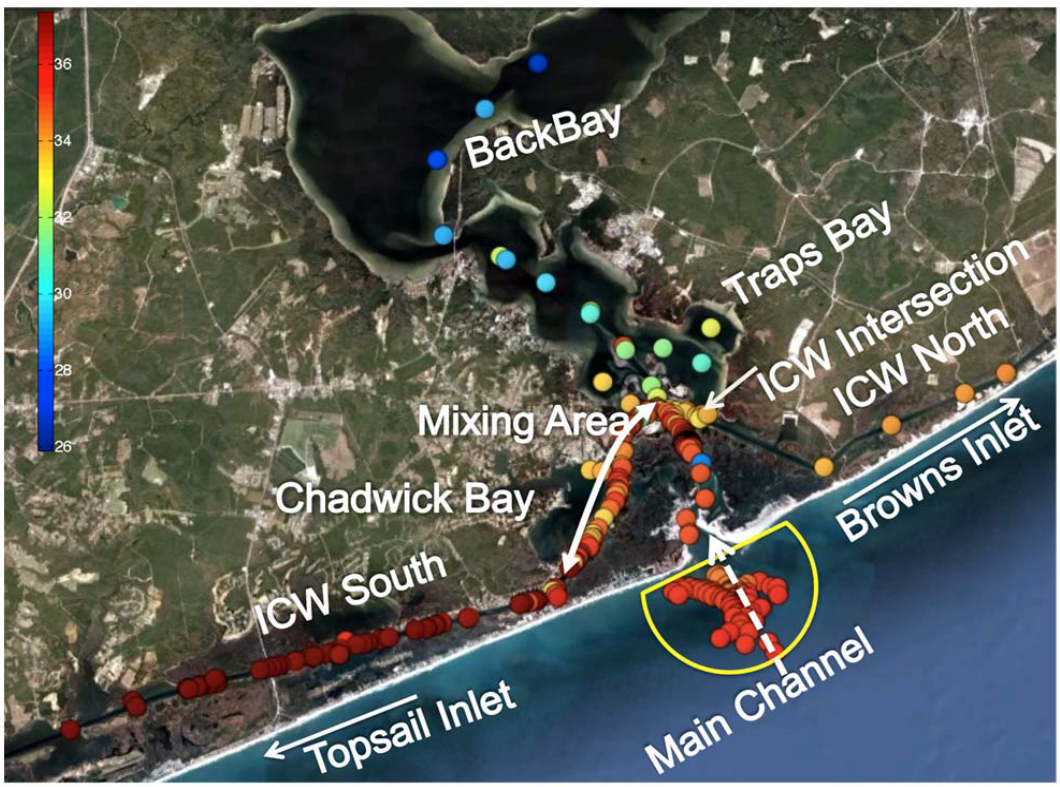

Figure 7. Google Earth Image of New River Inlet, NC. The main regions of the inlet system are outlined: main channel, backbay and the ICW north and south. The colored dots indicate the positions of the casts. The yellow semicircle represents the ebb delta. Colors denote depth-averaged salinity in psu, higher and lower values are represented by warmer and cooler colors, respectively.

6) Tidal Wave Reflection in Elkhorn Slough, CA

The shoreward and seaward propagating tidal wave signals for a short (11km) estuary were determined using four co-located pressure and velocity sensors longitudinally deployed in Elkhorn Slough,

Monterey Bay, CA to describe tidal wave reflection and distortion. Elkhorn Slough is a reflective (~100%) estuary consisting of a narrow (200m), gently sloping (1/4000) main channel with vast marshes and mud flats located along the channel. The amplitude reflection for the astronomical tidal constituents is ~90%. The amplitude reflection for tidal non-linearities, described by summing all non-astronomical tidal amplitudes, reflection is large (>125%) stating that the seaward tidal wave is more distorted than the shoreward tidal wave. It was found that the reflective time, defined as the time it takes the tidal wave to propagate to the landward boundary and back, increases as a function of tidal elevation (Figure 8). This is because the storage width associated with low-lying mud flats becomes more of factor in reducing the tidal phase-speed. The elevation-dependent reflective time caused by a depth-varying wave phase-speed distorts the shape of the seaward tidal wave relative to the shape of the shoreward tidal wave.

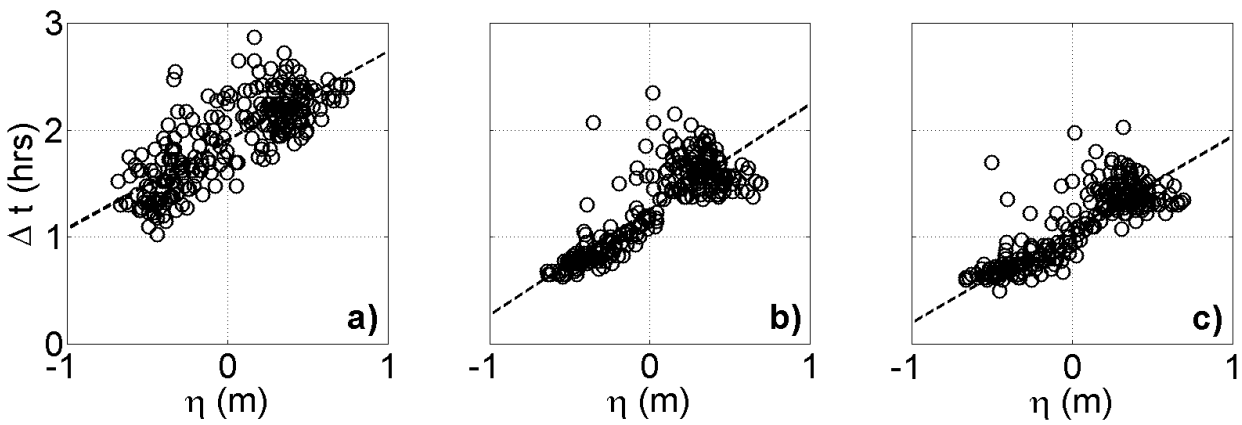

Figure 8. The reflective time lag estimated from daily high tide and low tide maxima and minima for three stations longitudinally deployed through the channel in Elkhorn Slough, CA. Dashed line represents the best-fit line estimated with linear regression. The linear slopes are 0.83, 0.99, and 0.87 and the R^2-values are 0.59, 0.69, and 0.60 for the three stations.

7) Rip-Current, Inner-Shelf Drifter Observations

Observations of rip current behavior outside the surf zone were obtained during a Rip current EXchange experiment (REX) in May 2009. Offshore waves measured in 13 m water depth, tidal elevation, and wind speed and direction were recorded throughout the experiment. Nine drifter deployments were conducted during varying wave and tidal conditions to measure surface current patterns. In an attempt to capture the spatial variation of rip-current flows that exit the surf zone, drifters were released using 3 approaches: 1) by swimmers in a cluster at the offshore edge of a rip channel, just outside of the surf zone, 2) by a boat in an alongshore line just outside of the surf zone, spanning 4-5 rip-channel/shoal systems, and 3) by a boat in a cross-shore line spanning from the edge of the surf zone and extending up to 2 surfzone widths offshore, in line with a rip channel. Conditions during the drifter deployments consisted of varying tidal stages, offshore waves with H_s of 0.38 to 1.49 m, T_p of 6.7 to 12.9 s, and approaching from the south, and winds blowing onshore with minimal wind stresses ($|\tau_s| < 0.05$ N/m^2).

In general, the drifters released outside the surf zone initially moved seaward due to rip currents and eventually returned shoreward in an arcing pattern, at times re-entering the surf zone over shoals, with no drifters being permanently removed from the nearshore region (Figure 8-9). The drifters typically

moved two to three surfzone widths seaward before returning shoreward, with a maximum cross-shore extent of six surfzone widths. Two distinguishable drifter patterns were observed: 1) the drifters moved seaward and returned sharply back shoreward a short alongshore distance from where they exited, resulting in locally contained cross-shore exchange, and 2) the drifters moved seaward and travelled farther in the alongshore direction as they gradually moved shoreward, resulting in cross-shore and alongshore exchange. Times of locally contained cross-shore exchange occurred when the rip currents were stronger during low tides and the alongshore currents outside the surf zone were weak. On yearday 122, at different times during the deployment, drifters were observed to move shoreward and seaward at about the same location offshore of a rip channel (y=250 m, x=200 m), depending on if the rip was pulsing at that time (Figure 8). Interestingly, on yearday 132, drifters that were moving shoreward outside the surf zone were pushed back offshore when they reached y=-200 m (offshore of a rip channel), due to a neighboring pulsing rip current; the drifters again moved seaward and north, then returned shoreward within 200 m in the alongshore (Figure 8). Times of cross-shore and alongshore exchange occurred when the rip currents were weak during high tides and the alongshore current outside the surf zone was stronger (Figure 9).

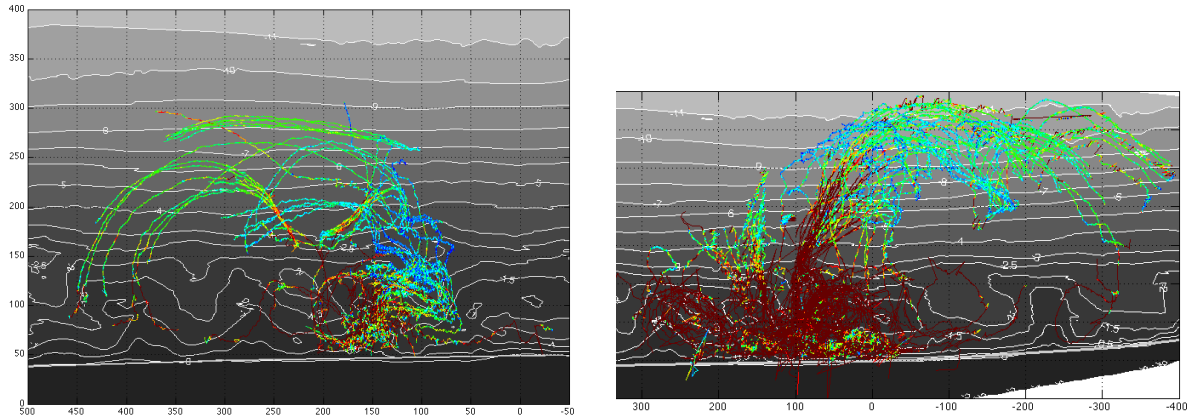

Figure 8. Examples of drifter position tracks during times of locally contained cross-shore exchange; (left) yearday 122, and (right) yearday 132. Color of line represents drifter speed.

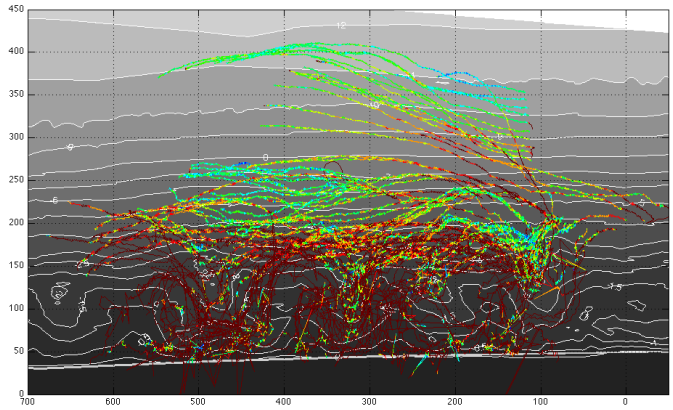

Figure 9. Example of drifter position tracks during times of cross-shore and alongshore exchange. Color of line represents drifter speed.

The behavior of the drifters moving offshore and onshore was evaluated by examining the drifter cross-shore velocity magnitudes as a function of cross-shore location (Figure 10). The study area was divided into 20m bins in the cross-shore direction, and the offshore and onshore moving drifters in each bin were averaged separately over the entire alongshore distance. Outside the surf zone, the offshore and onshore drifter velocity magnitudes are relatively equal. On days where there was more

alongshore exchange outside of the surf zone (yeardays 125, 126, 130, and 137), the offshore drifter velocities were slightly larger than the onshore drifter velocities due to the drifters moving quickly offshore in rip pulses but moving predominantly alongshore as they gradually moved onshore. The drifter cross-shore velocity magnitudes tended to be large at the edge of the surf zone and decrease with increasing distance away from the surf zone. The drifters outside the surf zone moving onshore demonstrate an increase in velocity magnitude as they approach the edge of the surf zone. The onshore moving drifters are actually accelerating as they re-enter the surf zone over shoals. These results differ from those of Ohlmann et al. [2012], who observed a tendency for drifters released on the inner shelf to decelerate as they moved shoreward on beaches that do not typically support rip currents. The drifter cross-shore velocity magnitudes are greater than the Stokes drift velocity estimates as a function of cross-shore location. Therefore, the return of the drifters onshore is not solely due to the net onshore Stokes drift due to waves.

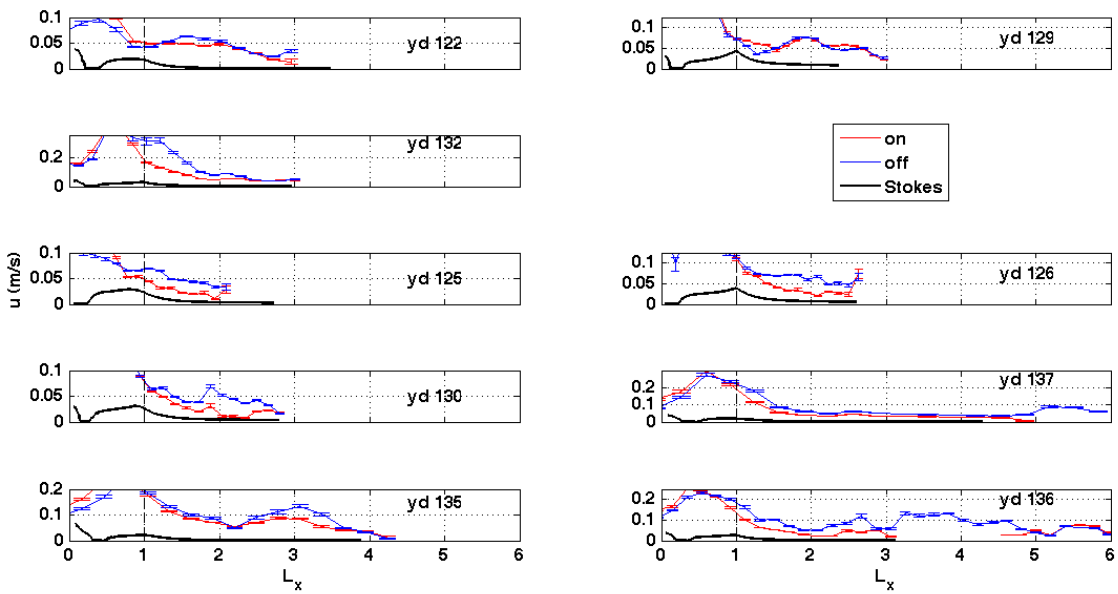

Figure 10. Cross-shore velocity magnitude as a function of cross-shore distance measured in surfzone-widths (L_x).

8) NPS-RSMAS Kootenai River Research: Riverine flow observations and modeling: sensitivity of Delft3D river model to bathymetric variability (UM no-cost extension).

The key element of this effort is to establish the sensitivity of river flow to (changes) in the bathymetry. All the relevant data have been collected in 2010 and two papers have been published (Brown et al., 2011 and MacMahan et al., 2012). At present we are working on finalizing three manuscripts: 1) *Spatially Variability of Natural River Mixing* by Swick et al., 2013. 2) *Numerical Model Comparisons of Transverse Mixing in a Natural River* by Swick et al., 2013 which will be submitted shortly.

IMPACT/APPLICATIONS

Overall the observations are important for understanding nearshore, riverine, and estuarine processes by providing high-quality data for numerical model validation. The model validation and verification have illuminated the effects of turbulence modeling, bed shear stress formulations, mixing and 3D flow

on tidal, riverine and nearshore Delft3D flow predictions. The use of the Delft3D model to design experiments and prepare drifter deployments has been extremely helpful and is a valuable finding for operational use.

The nonlinear coupling between high frequency tidal motions and low frequency motions is important to the subtidal and fortnightly backbay response. The subtidal and fortnightly motions transport colder, saline ocean water into the backbay, and increase sea levels in the estuary, and thus the nonlinear coupling between tidal constituents must be considered to predict the subtidal and fortnightly exchange of waters between the backbay and ocean. With modeling it has been shown that the 3D structure of the flow is important in controlling the maximum ebb velocities and therefore the tidal exchange between ocean and inlet affecting salinity and temperature variations and associated acoustic properties.

The geometric confirguration of the New River Inlet estuary and the proximity of the neighboring inlets influence the spatial characteristics of the optical and water properties. There are signifcant variations in these properties that occur within relatively short distances. The differences in the water masses were found to be important for the development of the confluence-type tidal instrusion fronts, which were observed for the first time at New River Inlet, NC. The mechanisms responsible for the instrusion front were succesfully analyzed with Delft3D modeling prior to the field experiment to optimize our instrument deployments.

There is a bit of uncertainity in the literature about the tidal behavior in short estuaries. The new observations in short Elkorn Slough estuary will provide the correct understanding of the tidal response for predictive capabilities.

The drifter response within the nearshore highlight that there is epsodic exchange between the surf zone and inner shelf. However, this mixing is limited to with a few surfzone widths from the shoreline.

We developed new inexpensive portable platforms (e.g. drifters and catamarans) that can easily be deployed from small vessels.

PUBLICATIONS (2012-2013) acknowledging ONR support

MacMahan, J., J. van de Kreeke, A.J.H.M. Reniers, S. Elgar, B. Raubenheimer, E. Thornton, M. Weltmer, P. Rynne, J.A. Brown (2013) Fortnightly tides and subtidal motions in a choked inlet, *in revision for Estuarine, Coasts and Shelf Sciences.*

MacMahan, J., C. Gon, and E.B. Thornton (2013) Tidal wave reflection and distortion is Elkhorn Slough, CA., *in revision for Estuarine, Coasts and Shelf Sciences.*

Weltmer, M.A., J.H. MacMahan, and A.J.H.M. Reniers (2013), Balance and control: Model simulations of tidal intrusion fronts in an idealized basin, *in prep. for Estuarine, Coastal, and Shelf Science.*

Weltmer, M.A., J.H. MacMahan, A.J.H.M. Reniers, E.B. Thornton, P. Rynne, and J. Brown (2013), Stratified confluence fronts in a shallow coastal plain estuary *in prep. for Journal of Geophysical*

Research.

Cited References

Brown, J., C. Tuggle, J. MacMahan, A. Reniers (2011), The use of autonomous vehicles for spatially measuring mean velocity profiles in rivers and estuaries, *Intelligent Service Robotics.* doi: 10.1007/s11370-011-0095-6

Faria, A.F., E. B. Thornton, T. P. Stanton, C. V. Soares, T.C. Lippmann, 1998. Vertical profiles of longshore currents and related bed shear stress and bottom roughness, J. Geophysical Research, Vol. 103, No. C2, pp 3217-3232

Hill, A.E., 1994. Fortnightly tides in a lagoon with variable chocking. Estuarine, Coastal, and Shelf Science 38, 423-434.

Keulegan, G.H., 1967. Tidal flow in estuaries, water level fluctuations of basins in communication with seas. Comm. On Tidal Hydraul., Army Corps of Eng., Vicksburg, Miss., Tech. Bull. 4, pp 89.

Kjerfve, B., Knoppers, B.A., 1991. Tidal-choking in a coastal lagoon, in Tidal Hydrodynamics, edited by B. Parker, John Wiley, N.Y., pp. 169-181.

Largier, J.L., 1992. Tidal intrusion fronts. *Estuaries*, 15, pp 26-39.

MacMahan, J., A. Reniers, W. Ashley, E. Thornton (2012) Frequency-Wavenumber Velocity Spectra, Taylor's Hypothesis and Length-Scales in a Natural Gravel-Bed River, *Water Resources Research* doi:10.1029/2011WR011709

Stigebrant, A., 1980. Some aspects of tidal interactions with fjord constrictions. Estuarine, Coastal, and Shelf Science. 11, 151-166.

Uittenbogaard, R.E., 1998. Model for eddy diffusivity and viscosity related to sub-grid velocity and bed topography. Note, WL | Delft Hydraulics.